1 **Does the molecular and metabolic profile of human granulosa cells correlate with oocyte fate?**

2 **New insights by Fourier transform infrared microspectroscopy (FTIRM) analysis**

3

4

5

6 Giorgia Gioacchini[1], Valentina Notarstefano[1], Elena Sereni[2], Carlotta Zacà[2], Giovanni Coticchio[2],

7 Elisabetta Giorgini[1], Lisa Vaccari[3], Oliana Carnevali[1], Andrea Borini[2]*

8 [1] Department of Life and Environmental Sciences, Polytechnic University of Marche, Via Brecce

9 Bianche 60131 Ancona, ITALY

10 [2]9.baby, Family and Fertility Center, Via Dante 15 - 40125 Bologna, ITALY

11 [3] SISSI Beamline, Elettra-Sincrotrone Trieste S.C.p.A., S.S.14 -Km 163.5, 34149 Basovizza,

12 Trieste, ITALY

13

14 * Corresponding author

15 Correspondence: borini@9puntobaby.it

16

17

18

19

20 **Running title:** Vibrational characterization of human granulosa cells

21

22

23

24

25

26

27

28

29

30

31

32

33

35

36

37

38   **Abstract**

39   **STUDY QUESTION**

40   Does the molecular and metabolic profile of human mural granulosa cells (GCs) correlate with

41   oocyte fate?

42   **SUMMARY ANSWER**

43   A close relation between the metabolic profile of mural GCs and the fate of the corresponding

44   oocyte was revealed by the analysis of selected biomarkers defined by GC Fourier transform

45   infrared microspectroscopy (FTIRM) analysis

46   **WHAT IS KNOWN ALREADY**

47   In ART, oocyte selection is mainly based on the subjective observation of its morphological

48   features; despite recent efforts, the success rate of this practice is still unsatisfactory. FTIRM is a

49   well-established vibrational technique recently applied to evaluate oocytes quality in several

50   experimental models, including human.

51   **STUDY DESIGN, SIZE, DURATION**

52   GCs retrieved from single-follicle aspirates were obtained with informed consent from 55 women

53   undergoing controlled ovarian stimulation for IVF treatment. GCs were analysed by FTIRM to

54   retrospectively correlate their spectral features with the fate of the companion oocytes. The study

55   has been conducted between March 2016 and September 2017.

56   **PARTICIPANTS/MATERIALS, SETTING, METHODS**

57   Patients were selected according to the following inclusion criteria: age <40 years; non-smokers; no

58   ovarian infertility diagnosis (only tubal, idiopathic and male infertility); regular ovulatory menstrual

59   cycles (25-30 days) with FSH < 10 IU/l on day 3 of the menstrual cycle; sperm sample with a total

60   motility count after treatment ≥ 300.000; number of retrieved oocytes ≥ 8.

61   Based on the clinical outcome of the corresponding oocyte, GCs were retrospectively classified into

62   the following experimental groups: clinical pregnancy (CP), fertilization failure (FF), embryo

63   development failure (EDF), and implantation failure (IF). All samples were analysed by the FTIRM

64   technique. The spectral biomarker signature of different oocyte fates was derived by several feature

65   selection procedures ('Leave-one-out' method on factorial discriminant analysis (FDA), variable

66   characterization method, and logistic regression method with the multinomial Logit model).

67   ANOVA, permutational multivariate ANOVA, FDA, and canonical analysis of principal co-

68   ordinates statistical tools were also applied to validate the identified spectral biomarkers.

MAIN RESULTS AND THE ROLE OF CHANCE

In total, 284 GCs samples were retrieved and retrospectively classified as FF: (N= 92), EDF (N= 113), IF (N= 56), and CP (N= 23). From the spectral profiles of GCs belonging to CP, FF, EDF and IF experimental groups, 17 spectral biomarkers, were identified by several feature selection procedures ($p < 0.0001$). These biomarkers were then validated by applying multivariate tools, to evaluate their ability to segregate GCs samples into the four experimental groups. FDA showed a clear separation along the F1-axis (62.75% of discrimination) between GCs from oocytes able (CP, IF groups) or not (FF, EDF groups) to develop into embryos; the F2-axis (24.14% of discrimination) segregated the embryos that gave pregnancy (CP) from those that failed implantation (IF). The confusion matrix (total percentage of correctness=80.25%) obtained from this analysis pinpointed that GCs from oocytes unable to develop into embryos (FF, EDF) were better characterized than those from oocytes able to give viable embryos (CP, IF). ANOVA ($p < 0.05$) analysis pinpointed that: each experimental group showed specific macromolecular traits, ascribable to different biological and metabolic characteristics of GCs; these metabolic features were likely associated with different oocytes fates, but not to patient characteristics, since from the same patient we obtained GCs with different metabolic profiles.

LIMITATIONS, REASONS FOR CAUTION

The study is based on a small sample size but provides proof of concept that the GCs' metabolic profile is associated with the companion oocyte fate. The generated model should be further tested on a larger cohort of patients, classified in a similar manner, to assess the potential predictive value of this approach. Ultimately, validity of the proposed approach should be tested in a RCT.

WIDER IMPLICATIONS OF THE FINDINGS

For the first time, the FTIRM analysis of human GCs has demonstrated an approach to better understand the molecular crosstalk between follicular cells and oocytes and has identified potential spectral biomarkers for improving human IVF success rate.

STUDY FUNDING/COMPETING INTEREST(S)

The study was funded by GFI grant. The authors declare that there is no conflict of interest.

Introduction

In the clinical routine of ART, oocyte selection is mainly based on the morphological features of its cytoplasm, polar body and cumulus cells (Balaban and Urman, 2006). All these criteria for grading and screening oocytes are subjective and controversial, and seem not to be related to the intrinsic competence of the oocyte (Serhal *et al.*, 1997; Balaban *et al.*, 1998; Guerif *et al.*, 2010; Ruvolo *et al.*, 2013). Moreover, the current knowledge of the mechanisms determining oocyte quality is still insufficient: what is known is that the relationship between the oocyte and its surrounding somatic cells is more complex than previously thought, and represents a determining factor for later developmental competence, crucial for the success of ART procedures (Suh *et al.*, 2002). In this light, the improvement of the oocyte quality assessment must be considered as critical to achieve higher success rates in ART. Helpful information can derive from the study of granulosa cells (GCs), which play a dominant role in regulating the development and competence acquisition of the oocyte and in maintaining the microenvironment as appropriate (Kidder and Vanderhyden, 2010). In fact, it is well known that the process of acquisition of oocyte competence, defined as the ability of an oocyte to be fertilized and to develop to the blastocyst stage, strictly depends on the follicular microenvironment (Al-Edani *et al.*, 2014) . All the processes involved in folliculogenesis heavily rely upon bi-directional interactions between germ cells and the surrounding GCs (Kidder and Vanderhyden, 2010). GCs are known to support oocyte growth (Brower and Schultz, 1982), control the advance of meiosis steps (Eppig, 1991), and regulate the oocyte transcriptional activity (De La Fuente and Eppig, 2001). Furthermore, GCs carry out these important functions through the production of steroid hormones such as estradiol and progesterone (Canipari, 2000), and of essential nutrients for oocyte development, modulating carbohydrate metabolism, and lipid synthesis, oxidation and storage in lipid droplets (Canipari, 2000; Chronowska, 2014). Hence, oocyte quality is strongly related to GC functions, and the identification of specific molecular markers related to the activity of these cells could be potentially used to predict oocyte quality (Uyar *et al.*, 2013).

Fourier transform infrared microspectroscopy (FTIRM) is a well-established vibrational technique, widely applied to various biomedical fields in life sciences for diagnostic purposes (Baker *et al.*, 2014). The coupling of infrared spectroscopy with visible light microscopy offers the possibility to detect, at the same time and on the same sample, unique chemical and biological information about the composition and the structural building blocks of the sample (Matthäus *et al.*, 2008; Movasaghi *et al.*, 2008). In fact, the analysis of FTIR spectral bands in terms of position, intensity and width, makes it possible to detect functional groups, bonding types and conformations of the most relevant biological molecules (proteins, lipids, sugars and nucleic acids) (Wolkers and Oldenhof, 2010).

134 Several studies have been already carried out on the FTIR analysis of female gametes (Giorgini *et*
135 *al.*, 2014). In a previous work, we obtained, for the first time, the infrared molecular fingerprint of
136 human oocytes retrieved from patients of different age: alterations in plasma membrane, protein
137 pattern, nucleic acids and metabolic processes were observed in oocytes from older patients
138 (Gioacchini *et al.*, 2014). An attempt to correlate the metabolomic profile of spent culture media by
139 near infrared spectroscopy with embryo viability in frozen–thawed embryo transfer cycles was also
140 carried out (Vergouw *et al.*, 2011).

141 Considering the successful biomedical application of these spectroscopic techniques and the need
142 for biological information not affected by the clinic environment and user manipulation, we
143 performed, for the first time, the FTIRM analysis of human GCs. The study aimed to define the
144 macromolecular and metabolic profile of single-follicle luteinized GCs; and retrospectively
145 correlate these spectral data to the companion oocyte fate (in terms of clinical pregnancy (CP),
146 fertilization failure (FF), embryo development failure (EDF), and implantation failure (IF)).

147

148 **Materials and Methods**

149

150 The study was approved by the Ethic Committee of 9.baby - Family and Fertility Center (Bologna,
151 Italy) and was carried out in full accordance with ethical principles, including The Code of Ethics of
152 the World Medical Association (Declaration of Helsinki) for experiments involving humans.
153 Approval for the study was obtained from the local Institutional Review Board. Selected patients
154 signed a written informed consent before participation to the study, which included the donation of
155 GCs.

156

157 *Patient selection*
158 The study included 55 couples attending 9.baby - Family and Fertility Center (Bologna, Italy) for
159 ART. Women were selected on the basis of the following inclusion/exclusion criteria: no smoking
160 habit, age <40 years, number of retrieved oocytes ≥8, diagnosis of tubal or idiopathic infertility,
161 regular menstrual cycles (25-30 days), and FSH levels < 10 IU/I on Day 3 of menstrual cycle. Male
162 partners had a sperm total motile count after treatment ≥ 300.000/ml.

163

164 *Ovarian stimulation protocol*
165 Controlled ovarian stimulation (COS) was induced using a GnRH agonist (Enantone, Takeda,
166 Rome, Italy) or an antagonist (Cetrotide, Serono, Rome, Italy; or Orgalutran, Organon, Rome, Italy)
167 and recombinant or urinary FSH (Gonal-F, Serono, Rome, Italy or Meropur, Ferring, Milan, Italy,

168 respectively). A dose of 10,000 IU hCG (Gonasi, Amsa, Rome, Italy) or one ampoule of

169 recombinant hCG (Ovitrelle, Serono, Rome, Italy) was administered to achieve final oocyte

170 maturation when one or few follicles reached a maximum diameter of >23 mm. Oocyte collection

171 was performed transvaginally, under ultrasound guidance, 36 h after hCG injection.

172

173 *GC sample collection*

174 GCs were obtained from single-follicle aspirates of oocytes retrieved. Follicular fluid was

175 centrifuged at 1100x g for 10 min at room temperature. The supernatant was discarded and the

176 pellet was dissolved in 2 mL of Sydney IVF Gamete Buffer Medium (Cook IVF, Brisbane,

177 Australia) and overlaid on a 80%-40% discontinuous gradient of silica particles suspension (1 mL

178 PureSperm 40 and 1 mL PureSperm 80; Nidacon, Goteborg, Sweden) and centrifuged at 1600x g

179 for 13 min at room temperature. After centrifugation, three layers were observed: a top layer

180 containing the follicular fluid, a middle ring-like layer containing GCs and a bottom layer

181 containing erythrocytes. GCs were recovered from the middle ring-like layer using a Pasteur pipette

182 and placed into 1 mL of NaCl 0.9% solution (Fresenius Kabi, Bad Homburg, Germany). In the

183 presence of contaminating red blood cells after initial isolation, a second step of gradient separation

184 was repeated. Isolated GCs were centrifuged at 300x g for 10 minutes. The supernatant was

185 discarded and the pellet re-suspended in 1 mL of NaCl 0.9% solution and washed again at 300x g

186 for 10 minutes. After additional centrifugation for 5 min at 600x g, the cell pellet was re-suspended

187 in 100 μl of sterile NaCl 0.9% solution. All centrifugations were carried out at room temperature.

188 Before infrared (IR) measurements, all samples were first screened by transmitted light microscopy

189 to verify possible gross contamination by cumulus cells (CC). Moreover, in order to rule out the

190 presence of residual CC in the samples, we performed the FTIRM characterization of both CCs and

191 GCs, obtaining two very different and well discernable spectral profiles that were used to confirm

192 the purity of the samples analysed in the study. Samples contaminated by CCs were discarded.

193

194 *Oocytes culture, insemination, embryo culture and transfer*

195 Oocytes were collected, rinsed and placed individually in 50 ☐l drops of Sydney IVF Fertilization

196 Medium (Cook IVF, Brisbane, Australia) at 37 °C, 6 % CO_2, 5 % O_2 e 89 % N_2 until insemination.

197 From this step on, every oocyte was cultured and handled singly until the embryo transfer to

198 confirm its perfect correspondence with its own follicular fluid and in turn with its own granulosa

199 cells.

200 Semen preparation procedures and ICSI were carried out as previously described (Borini *et al.*,

201 1996).

202 Approximately 40 hours after hCG administration, the oocytes were inseminated by standard ~~the~~

203 ~~conventional~~ IVF (22 patients) or ICSI (33 patients) technique.

204 At 16–18 h after insemination (Day 1), normal fertilization was assessed by observing the presence

205 of two pronuclei and zygotes were placed in fresh Sydney IVF Cleavage Medium (Cook IVF,

206 Brisbane, Australia). Embryo culture was carried out in an Embryoscope (UnisenseFertiliTech,

207 Denmark), an integrated embryo-culture time-lapse microscopy system, in a $N_2/CO_2/O_2$ (89:6:5,

208 v/v) atmosphere at 37°C without control of humidity. On Day 3, embryos were transferred into

209 Sydney IVF Blastocyst Medium (Cook IVF, Brisbane, Australia) and cultured until Day 5 or Day 6.

210 Transfer of a single blastocyst was performed on Day 5 or on Day 6. Blastocysts were evaluated on

211 the basis of the degree of expansion, and quality of inner cell mass and trophectoderm cells, as

212 described in the modified Gardner and Schoolcraft grading system by Cornell's group (Veeck and

213 Zaninović, 2003).

214 Clinical pregnancy was confirmed by both high levels of hCG and ultrasound detection of a

215 gestational sac.

216 Supernumerary blastocysts were individually cryopreserved using a vitrification protocol (Kitazato

217 BioPharma Co, Japan) with a closed-system device (HSV straw, Cryo Bio System, France) as

218 previously described (Cobo *et al.*, 2008).

219

220 *Experimental design*

221 In total, 284 GCs samples retrieved from the 55 enrolled patients were retrospectively classified

222 according to the corresponding oocyte clinical outcome into the following experimental groups:

223 **FF**: GCs from oocytes that failed to support a normal fertilization, (N= 92).

224 **EDF**: GCs from oocytes developing into embryos that arrested during culture between day 2 and

225 the time of transfer (day 5 or day 6), (N= 113).

226 **IF**: GCs cell from oocytes developing into good quality embryos that failed to implant after

227 transfer, (N= 56).

228 **CP**: GCs from oocytes developing into good quality embryos that gave rise to a clinical pregnancy

229 after transfer, (N= 23).

230 The methodological process of the study is sketched in Figure 1.

231

232 *FTIRM data collection*

233 The FTIRM analysis was carried out at the infrared beamline SISSI (Synchrotron Infrared Source

234 for Spectroscopic and Imaging), Elettra-Sincrotrone Trieste, Italy. A Hyperion 3000 Vis-IR

235   microscope equipped with a nitrogen-cooled HgCdTe detector (MCT_A) and coupled with a Vertex

236   70 interferometer (Bruker Optics GmbH, Ettlingen, Germany) was used.

237   The GC suspensions (10 μL each, at ~10^5 cells/ml) were dropped with a Gilson pipette onto CaF_2

238   UV grade optical windows for IR analysis (38.0x26.0x1.0 mm, Crystran Ltd.) and then left to dry at

239   room temperature under a biological hood for 30 minutes. For each GC sample, 30 zones with

240   dimensions of 30x30 μm containing densely packed cell monolayers were selected by visible

241   microscopy. On these areas the corresponding IR spectra were acquired in transmission mode, with

242   a conventional GlowBar source. A 15X Schwarzschild objective (NA=0.4, working distance=24

243   mm) matched with a 15X condenser in the Mid-IR region were used. Each spectrum was collected

244   with a spectral resolution of 4 cm^{-1} in the IR spectral range 4000-800 cm^{-1} and was the result of an

245   average of 256 scans. A background spectrum was collected before each sample analysis on a clean

246   zone of the optical window.

247

248   *Pre-processing procedure of IR spectra*

249   All the absorbance IR spectra acquired were corrected for water vapour and CO_2 contributions by

250   running the Atmospheric Compensation routine of OPUS software, and vector normalized in the

251   entire spectral range, to mitigate for non-homogeneous thickness of samples (OPUS 7.1 software,

252   Bruker Optics GmbH, Germany). Spectra were then cut in the spectral range 4000-1191 cm^{-1} owing

253   to the possible presence, at lower wavenumbers, of bands related to contaminants used during the

254   GC collection step.

255   To discard outliers, all the spectra acquired for each sample were analysed as follows. The areas of

256   the 2990−2899 cm^{-1} and 1775−1191 cm^{-1} spectral intervals were calculated by drawing a straight

257   line between the aforementioned wavenumber limits and integrating the area above this line

258   (Integration Mode B, OPUS 7.1 software); their sum was defined as the overall cellular

259   biomolecular content (Cell). For each GC sample, the mean of Cell ± SD was calculated, and all the

260   spectra with values outside this range were discarded. Only those GC samples with at least 15

261   remaining spectra were further analysed.

262

263   *IR data analysis*

264   On each IR spectrum, specific bands of biological relevance were identified. For each of them, the

265   corresponding spectral interval and the assignment to specific cellular functional groups were

266   reported (Table I). Then, for all these bands, the area integrals were obtained by using the

267   aforementioned Integration Mode B and used to calculate specific band area ratios (Table II).

268

Biomarker signature

For the biomarkers signature a balanced dataset, named DS1, was built. For this purpose, due to the different size of each experimental group (**CP,** N=23; **FF**, N=92; **EDF**, N=113; **IF**, N=56), not all the analysed GC samples were used; in particular, all the **CP** GCs (N=23) were selected, while for **FF**, **EDF** and **IF** GCs, only 23 samples were randomly selected, respectively. The validation of this random selection was performed by exchanging, one by one, the samples included in the dataset with others belonging to the same experimental group (data not shown). Approximately, for each patient, two samples belonging to different experimental groups were chosen, for a total of 92 GC samples. DS1 was composed of 1043 rows, corresponding to the IR spectra of these selected GCs samples (290 for **CP**, 286 for **FF**, 200 for **EDF**, and 267 for **IF**), and 19 columns corresponding to all the band area ratios calculated on these IR spectra and reported in Table II.

To identify the minimal subset of band area ratios (feature selection) necessary and non-redundant to segregate and characterize the experimental groups **CP**, **FF**, **EDF**, and **IF** (defined as biomarker signature), the following statistical approaches were carried out on DS1 (XLSTAT 2017.01, Addinsoft, New York, NY, USA): *'Leave-one-out' method on FDA (Factorial Discriminant Analysis)*: FDA was performed by using all the band area ratios in DS1 and removing them one at a time, to evaluate their relevance in the definition of the experimental groups; *Variable Characterization method*: this method let us characterize the experimental groups, investigating the relations shared with the characterizing features: hence it provides information on whether a feature is necessary or not to describe the experimental groups. To this end, a correlation coefficient is calculated between the categorical variable to characterize (experimental group) and the characterizing feature (band area ratio): if this coefficient is different from 0, a significant dependence exists between the categorical variable (experimental group) and the features (band area ratios). The statistical significance was determined by the Fisher F-test ($p < 0.05$); *Logistic Regression method with the Multinomial Logit model:* this method was performed to link a set of selected features (band area ratios) with the probability of occurrence/non-occurrence of an event (the probability that a GC sample belongs to one of the experimental groups), after classifying the features according to their importance and usefulness to distinguish the experimental groups. The null hypothesis (H0) was tested to define whether the variables (features) bring significant information: in particular, the Likelihood ratio test (-2 Log(Likelihood)), the Score test and the Wald test were performed comparing the model (built on the basis of DS1, composed of observations divided into experimental groups and features) with a simpler model composed of only one given constant. In addition, to determine whether all the selected features bring significant information, a further check was performed, running the Likelihood ratio test and removing one

303 feature at a time: if Pr > LR (where Pr is the probability and LR is the likelihood ratio Chi square) is

304 smaller than a selected significance threshold (*p* value 0.05), then the feature is necessary to

305 describe the group.

306

307 *Biomarker validation*

308 To validate the selected biomarkers two multivariate statistical analyses were performed on a new

309 dataset, named DS2, composed of 1043 rows, corresponding to the IR spectra on which band area

310 ratios were calculated (290 for **CP**, 286 for **FF**, 200 for **EDF**, and 267 for **IF**) and of 17 columns,

311 corresponding to the 17 spectral biomarkers selected. In particular, permutational multivariate

312 ANOVA (PERMANOVA) and factorial discriminant analysis (FDA) (Primer-E, Plymouth, UK)

313 were carried out by using DS2. PERMANOVA is a distribution- and parameter-free multivariate

314 analysis of variance, which uses permutations to estimate the statistical significance

315 (PERMANOVA+ add-on package of the PRIMER-E software v. 6, Plymouth, UK,). The data

316 included in DS2 were normalized and organized in a Euclidean-distance matrix; the number of

317 permutations was always set at 999. Statistical significance was set at 0.05 and was evaluated by the

318 *p* value obtained by the permutation procedure for each term, named P(perm) (Anderson, 2001),

319 and by the Monte Carlo random draws from the asymptotic permutation distribution, named P(MC)

320 (Anderson and Robinson, 2003). A pair-wise PERMANOVA was also performed to carry out a

321 one-to-one correlation of all the experimental groups.

322 FDA enabled determination of which biomarkers were useful and necessary to discriminate GCs

323 previously classified into the experimental groups (XLSTAT 2017.01, Addinsoft, New York, NY,

324 USA). Statistical significance was set at $p < 0.05$. The null hypothesis (H0) that the within-class

325 covariance matrices are equal was evaluated by the Box's test (carried out both with chi-square and

326 Fisher's F asymptotic approximations) and the Kullback test. Wilks' Lambda test was also used to

327 reject the null hypothesis that the mean vectors of the experimental groups are equal.

328 In addition, to further strengthen the validation of biomarkers previously selected canonical analysis

329 of principal co-ordinates (CAP) was performed on a new dataset, named DS3. DS3 was built

330 including only the average values of the biomarkers for each GC sample, hence composed as

331 follows: n. 23 rows for **CP**, n. 23 rows for **FF**, n. 23 rows for **EDF** group, and n. 23 for **IF** group,

332 for a total of 92 rows and 17 columns, corresponding to the 17 spectral biomarkers selected. CAP is

333 a constrained ordination method, which tests for significant differences among the *a priori* defined

334 groups in multivariate space (PERMANOVA+ add-on package of the PRIMER-E software, v. 6,

335 Plymouth, UK), finding the axes through the multivariate cloud of points, which best separate the *a*

336 *priori* given groups (Anderson and Willis, 2003). The data included in DS3 were normalized and

organized in a Euclidean-distance matrix; the number of permutations was always set at 999. Pearson correlations were used to show linear relationships of spectral data with axes. The p value obtained using permutation procedures let us evaluate the *a priori* hypothesis of no difference within experimental groups. The value of the squared canonical correlation (δ_1^2) was used to assess the strength of the association between multivariate data and the hypothesis of group differences. A proper number of principal co-ordinates axes (m) was chosen automatically by the CAP routine. Lastly, a cross-validation procedure was performed for the chosen value of m (Anderson and Willis, 2003).

Macromolecular characterization of GCs belonging to different experimental groups

The DS2 dataset was submitted to ANOVA followed by Dunnett's multiple comparisons test to better understand and highlight the macromolecular and metabolic pattern characterizing GCs belonging to each experimental group (OriginPro, version 9.4, OriginLab, Northampton, MA, USA). Statistical significance was set at $p < 0.05$.

Results

Single-follicle aspirate GCs, obtained with informed consent from 55 women undergoing a COS for IVF treatment, were analysed, for the first time, by using FTIR microspectroscopy. GC samples were retrospectively classified asCP),FF, EDF, and IF

On IR spectra of each GC sample, the following band area ratios were calculated and related to the concentration and structure of meaningful biomolecules contained in GCs (see Table I and Table II)

Biomarker selection

The DS1 dataset, containing the 19 band area ratios calculated on all the IR spectra (N = 1043) acquired on GCs samples (N = 92), was used for the following feature selection procedures.

'Leave-one-out' method on FDA. FDA was performed both on DS1, including all the 19 band area ratios (features), and on other 19 datasets, obtained by removing from DS1 one feature at a time. Supplementary Table SI reports the total percentages of correctness of the classification obtained by comparing the results from all datasets. The correctness percentage of the classification was increased when excluding PH1/LIP (phosphate 1/lipids) and 1400/LIP. Conversely, for the remaining 17 investigated features, the total percentage of correctness was lower than the one achieved using all the band area ratios.

371

372   In the variable characterization method, the characterization of the categorical variable

373   'experimental group' was performed in order to elucidate the link it shared with the selected

374   features (band area ratios). In this light, the correlation coefficient was calculated between the

375   categorical variable and the characterizing feature, and then its value was analysed by Fisher F-test,

376   in order to identify a possible dependence existing between the categorical variable (experimental

377   group) and the features (band area ratios). For all the variables, the overall correlation coefficient

378   was significantly different from 0, except for 1400/LIP ($p = 0.243$) and PH1/LIP ($p = 0.367$)

379   (Supplementary Table SII).

380

381   The logistic regression with multinomial logit model method was performed to classify the features

382   according to their importance and usefulness for distinguishing the experimental groups. The null

383   hypothesis (H0) was tested to define if all the features bring significant information, by the

384   Likelihood ratio test (-2 Log(Likelihood)), the Score test and the Wald test: the model constructed

385   on the basis of DS1 was compared with a simpler model composed of only one given constant (H0:

386   Y= 0.274). Supplementary Table SIII reports the results of the three tests, in terms of probability of

387   the Chi-square test (Pr > Chi2) which is always lower than 0.0001, letting us conclude that

388   significant information is provided by the variables, and the model based on DS1 is more robust

389   than the one related to the null hypothesis.

390   In addition, to determine whether all the selected features bring significant information, the

391   Likelihood ratio test was performed removing one feature at a time: Pr > LR (where Pr is the

392   probability and LR is the Likelihood Ratio Chi Square) checked for each feature, was smaller than

393   0.05. Hence, all the features, except for PH1/LIP and 1400/LIP, are necessary to describe the model

394   (Supplementary Table SIV).

395   According to the results obtained by the three feature selection procedures ('Leave-one-out' method

396   on FDA, Variable Characterization method, and Logistic regression method with Multinomial Logit

397   Model), the following 17 features were selected as biomarkers and used to build a new dataset,

398   DS2: Lipids/overall cellular biomolecular content (LIP/CELL), Proteins/overall cellular

399   biomolecular content (PRT/CELL), AmideI/AmideII (AI/AII), Liids/Protiens (LIP/PRT),

400   Phospahate 1/ overall cellular biomolecular content (PH1/CELL), Phospahate 1/Proteins

401   (PH1/PRT), Carbonyl ester of fatty acids/ overall cellular biomolecular content (COO/CELL),

402   Carbonyl ester of fatty acids/Lipids (COO/LIP), 1400/Proteins 1400/PRT, 1460/Proteins

403   (1460/PRT), 1400/1460, 1460/Lipids (1460/LIP), Unsaturated alkyl chains of lipids/ overall cellular

404   biomolecular content (CH/CELL), Unsaturated alkyl chains of lipids/Lipids (CH/LIP), Unsaturated

405   alkyl chains of lipids/ Methyl groups of cellular lipids (CH/CH3), Methylene groups of cellular

406   lipids/Lipids (CH2/LIP), and Methyl groups of cellular lipids/ Methylene groups of cellular lipids

407   (CH2/CH3).

408

409   *Biomarker validation*

410

411   The PERMANOVA analysis indicated a strong discerning effect of the 17 selected biomarkers in

412   the segregation of GCs samples from **CP**, **FF**, **EDF**, and **IF** experimental groups (P(perm) = 0.001,

413   P(MC) = 0.001) (Supplementary Table SV). A pair-wise PERMANOVA was also performed to

414   compare all pairs of experimental groups. Table III provides pair-wise post-hoc test results, which

415   confirm a statistically significant discerning potential of the 17 selected biomarkers with respect to

416   **CP**, **FF**, **EDF**, and **IF** GCs.

417

418   The results obtained from the two Box's tests, carried out by using the chi-square asymptotic

419   approximation and the Fisher's F asymptotic approximation, and by the Kullback test

420   (Supplementary Table SVI), confirmed the need to reject the hypothesis that the covariance

421   matrices are equal among the groups.

422   The interpretation provided for the tests cited above, established that, as the computed *p* value is

423   lower than 0.05, the null hypothesis H0 that the within-class covariance matrices are equal, should

424   be rejected. F1 and F2 factors, with a cumulative discrimination percentage of 86.887, were used to

425   perform FDA. The plot describing how the 17 selected biomarkers correlate with F1 and F2 factors

426   is reported in Figure 2A.

427   GC samples were classified by testing the posterior probability of the observations to belong to one

428   of the experimental groups. The overall success of classification was of 80.25% (Table IV); in

429   particular, the confusion matrix resulting from the analysis reporting the percentage of well

430   characterized observations, showed that the best characterized group was **EDF** (88.50%), followed

431   by **FF** (84.97%), **IF** (78.65%) and then **CP** (71.38%).

432   The percentages were obtained dividing the number of well classified observations by the total

433   number of observations. Figure 2B shows the observations plotted on the factor axes.

434

435   CAP analysis was performed by using the DS3 dataset (see Materials and Methods). The plot

436   obtained by CAP routine, showing the segregation of the four experimental groups and the Pearson

437   correlations as vectors, is reported in Figure 3.

438   The cross-validation procedure assigned 69.565% of observations to **CP**, 73.913% to **IF**, 82.609%

439   to **FF** and 91.304% to **EDF**, with a total correctness of 79.348% (Table V).

440   Percentages of correctness were calculated dividing the number of well classified observations by

441   the total number of observations. The very large (0.82259) first squared canonical correlation, the *p*

442   value of 0.001, together with the high cross-validation allocation success, additionally indicate the

443   significance of the 17 selected biomarkers in segregating GC samples in the experimental groups.

444

445   *Macromolecular characterization of GCs from different experimental groups*

446

447   DS2 was submitted to the ANOVA test for analysing the statistical variance of selected biomarkers

448   among the experimental groups **CP**, **FF**, **EDF** and **IF**. The results are summarized in Figure 4. Each

449   group was characterized by specific levels of band area ratios, representative of different biological

450   and macromolecular traits. In particular, GCs from the **CP** experimental group showed lower values

451   of the CH2/CH3 and CH2/LIP ratios (Figure 4L, M), and higher values of the 1400/1460 ratio

452   (Figure 4H), indicating a high amount of long chain fatty acids and of branched lipid chains. In **FF**

453   GCs, higher values of LIP/CELL, CH/CELL, CH/LIP, and CH/CH3 ratios (respectively, Figure 4A,

454   I, J, K) were found, representative of an increment of lipids with unsaturated alkyl chains. GCs

455   from the **EDF** group showed higher values of PRT/CELL (Figure 4B) and lower values of

456   COO/CELL, COO/LIP and LIP/PRT (respectively, Figure 4D, E, P), indicating lower amounts of

457   lipids with respect to proteins; moreover, lower values of PH1/CELL and PH1/PRT (respectively,

458   Figure 4C, Q) were found suggesting a decrement of phosphate groups with respect to both the total

459   cellular and protein amounts. **IF** GCs were mostly characterized by higher values of COO/CELL,

460   COO/LIP and 1460/LIP (respectively, Figure 4D, E, N), suggesting higher amounts of fatty acids;

461   in addition, an increase of the 1400/PRT, 1460/PRT, AI/AII and LIP/PRT ratios (respectively,

462   Figure 4F, G, O, P) was detected, suggesting a lower amount of proteins with respect to lipid alkyl

463   chains.

464

465   **Discussion**

466

467   ART is a recognized medical practice leading to the birth of millions of babies, even if the success

468   rate of such practice is still unsatisfactory (Tarín *et al.*, 2014). Furthermore, Patrizio and Sakkas

469   stated that only approximately 5% of fresh oocytes retrieved in ART leads to the birth of a baby

470   (Patrizio and Sakkas, 2009), and it is still not known if the remaining 95% of retrieved oocytes

471   reflects "natural physiological waste" or if we are not able to correctly assess their quality.

472   In recent years, several studies have been conducted on the CC and GC transcriptome, their

473   metabolism and other functionalities, to identify molecular biomarkers of oocyte quality

474   (Adriaenssens *et al.*, 2010; Uyar *et al.*, 2013; Kim *et al.*, 2014; Dumesic *et al.*, 2015; Borup *et al.*,

475   2016; D'Aurora *et al.*, 2016; Kordus and LaVoie, 2017); however, there is a lack of consensus on

476   the achieved results (Uyar *et al.*, 2013).

477   In the present study, FTIRM was used for the first time, to characterize the vibrational fingerprint of

478   GCs from single-follicle aspirates. GC samples were collected from patients selected on the basis of

479   a specific set of inclusion/exclusion criteria, to avoid biases related to age (Broekmans *et al.*, 2009;

480   Tatone and Amicarelli, 2013), stimulation protocols (Hamamah *et al.*, 2006; Adriaenssens *et al.*,

481   2010; Haas *et al.*, 2014), smoking habits (Gannon *et al.*, 2013; Sadeu and Foster, 2013), and

482   infertility diagnosis (González-Fernández *et al.*, 2010). The spectral information from GCs was

483   retrospectively related to the corresponding oocyte clinical outcome, in terms of clinical pregnancy

484   (**CP**), fertilization failure (**FF**), embryo development failure (**EDF**), and implantation failure (**IF**),

485   and 17 spectral biomarkers were selected.

486   A strong discerning effect of these biomarkers was identified by PERMANOVA analysis, in terms

487   of segregation of GCs samples into **CP**, **FF**, **EDF**, or **IF** experimental group. In addition, the

488   analysis of the FDA scores plot highlighted a clear separation of **CP** and **IF** GCs from **FF** and **EDF**

489   GCs along F1 axis (62.75% of discrimination), and hence between GCs from oocytes that are able

490   or not able to develop into embryos. Furthermore, the F2 axis (24.14% of discrimination)

491   segregated **CP** from **IF** GCs, and hence embryos that resulted in a pregnancy from those that failed

492   implantation. These results are not surprising, because the oocyte contribution is relevant but not

493   exclusive considering also the role of the paternal contribution during the first stages of embryo

494   development. Moreover, the embryo implantation capability depends not only on the embryo itself

495   but also the endometrial receptivity of the patient.

496   The analysis of the plot describing how the 17 selected biomarkers correlate with F1 and F2 factors

497   is consistent with the results from ANOVA for almost all the biomarkers. In particular, **CP** GCs

498   were discriminated by the 1400/1460 ratio, COO/LIP, COO/CELL and 1460/PRT ratios were

499   discriminant for **IF** GCs, while CH/LIP and CH/CELL segregated **FF** GCs; finally, **EDF** GCs were

500   separated by PH1/PRT and PH1/CELL ratios. The confusion matrix reporting the percentage of

501   well classified observations, confirmed that GCs from oocytes unable to develop into embryos

502   (**EDF** and **FF**) were better characterized than those from oocytes able to give viable embryos (**IF**

503   and **CP**).

504   Finally, the results obtained from CAP analysis were consistent with those obtained from FDA,

505   demonstrating that the simplified dataset DS3 contains the fundamental information necessary for

506   the correct classification of GCs into the four experimental groups.

507   Different biological characteristics of GCs belonging to different experimental groups were

508   pinpointed by ANOVA analysis. Hence, these results confirm the close relation between oocyte fate

509   and the follicular microenvironment (Dumesic *et al.*, 2015), and shed new light on the specific

510   biochemical alterations in GCs and how they impact on the different clinical outcomes of their

511   companion oocytes. In particular, **FF** seemed to be associated with an impairment in GC lipid

512   metabolism, with higher amount of lipids and unsaturated alkyl chains. Among the main functions

513   of GCs, lipid metabolism, consisting of lipid oxidation and storage in lipid droplets, is a crucial

514   factor for correct follicle development (Gilchrist *et al.*, 2008). The utilisation of triglycerides and

515   fatty acids for metabolic needs relies on the lipolysis of triacylglycerol within lipid droplets,

516   necessary for oocyte development (Dunning *et al.*, 2014). Hence, our results suggest that GCs with

517   an impaired lipid metabolism could impair lipid storage of the surrounding oocyte thereby reducing

518   its ability to be fertilized.

519   In addition, GCs play a crucial role in regulating the pattern protein phosphorylation in the oocyte,

520   as proved by culturing oocytes with or without follicular cells (Colonna *et al.*, 1989; Cecconi *et al.*,

521   1991). The alteration in protein metabolism and the decrease in terms of phosphate groups in GCs

522   belonging to the **EDF** experimental group shown in this study, could suggest an alteration of

523   phosphorylated protein supply to the oocyte, resulting in a reduced ability of the oocyte to correctly

524   develop into embryo. A concomitant alteration in both lipid and protein metabolism characterized

525   by an increment of fatty acids and lower amount of proteins, as found in GCs from the **IF**

526   experimental group, could be related to an impairment in the capability of the oocyte to develop

527   into an embryo that can implant properly. Finally, from results concerning GCs belonging to **CP**

528   experimental group, it is evident that not only the correct amount of macromolecules supplied by

529   the GCs but also the quality (long chain fatty acid) could make the difference for the fate of the

530   surrounded oocyte.

531   All these results demonstrate that GCs belonging to different experimental groups are characterized

532   by specific macromolecular traits, ascribable to different biological and metabolic features.

533   Moreover, these metabolic differences of GCs are strictly correlated to the companion oocyte fate

534   and not to patient characteristics, and hence may explain why oocytes retrieved from the same

535   patient undergo different fates.

536   To conclude, this is a proof-of-concept study suggesting the potential of FTIRM to identify

537   biochemical differences in human GCs associated with oocytes with different developmental

538 destinies. As such, in the first place this initial finding should be validated with larger groups of
539 samples obtained from patients selected according to the same selection criteria. Then the
540 applicability of the identified biomarkers should be verified for samples derived from other patient
541 typologies, to assess the universality of the methodology. Ultimately, the clinical relevance of the
542 proposed approach should be tested in a RCT, before introduction into clinical practice (Harper et
543 al., 2012). Regardless, the identified and validated biomarkers could be the basis for the
544 development of a data standardization system based on machine learning techniques, with the final
545 step of establishing a reliable, non-invasive and objective tool to predict oocyte fate by analysing
546 the vibrational fingerprint of the surrounding GCs. Analysis of follicle cells as an approach to
547 oocyte assessment and selection, such as that illustrated in the present study, has considerable
548 potential advantages over more established embryo selection tools, for example preimplantation
549 genetic testing (PGT). In fact, while PGT is technically highly developed and widespread, it
550 requires removal of 1-2 blastomeres at the cleavage stage or 3-10 cells from the trophectoderm of
551 the blastocyst. It has been shown that subtraction of such material is significantly detrimental to
552 embryo viability at the cleavage stage. Concerns are also growing on the possibility that embryo
553 biopsy can affect the implantation potential of the blastocyst. On the contrary, methodologies based
554 on follicle cells analysis are totally non-invasive by definition and therefore promise to bring about
555 a leap in the quest for safe and efficient oocyte/embryo selection. It is important to note, however,
556 that any possible gamete/embryo selection tool, even if developed to a high level, can only improve
557 treatment efficiency, i.e. reduce the effort (e.g. time to pregnancy or the number of attempts in a
558 time interval) required to achieve a viable pregnancy. In contrast, increments in treatment efficacy
559 (e.g. overall rate of success) will require more innovative, and difficult to develop, approaches to
560 improvement of gamete or embryo quality.
561

562 **Authors' roles**

563 GG, EG, OC, and AB designed the experiments; ES and CZ conducted the GCs sampling; LV, GG,
564 EG and VN performed FTIR measurements; GG, EG and VN performed data analysis; GG, EG,
565 VN, AB, GC and OC wrote the paper.

566

569

570 **Conflict of interest**

571 The authors declare no competing interests.

572

573

574

575 **References**

576

577 Adriaenssens T, Wathlet S, Segers I, Verheyen G, Vos A De, Elst J Van der, Coucke W, Devroey
578   P, Smitz J. Cumulus cell gene expression is associated with oocyte developmental quality and
579   influenced by patient and treatment characteristics. *Hum Reprod* 2010;**25**:1259–1270.

580 Al-Edani T, Assou S, Ferrières A, Bringer Deutsch S, Gala A, Lecellier CH, Aït-Ahmed O,
581   Hamamah S. Female aging alters expression of human cumulus cells genes that are essential
582   for oocyte quality. *Biomed Res Int* 2014;**2014**:1–10.

583 Anderson MJ. A new method for non-parametric multivariate analysis of variance. *Austral Ecol*
584   2001;**26**:32–46.

585 Anderson MJ, Robinson J. Generalized discriminant analysis based on distances. *Aust New Zeal J*
586   *Stat* 2003;**45**:301–318.

587 Anderson MJ, Willis TJ. Canonical analysis of principal coordinates: a useful method of contrained
588   ordination for ecology. *Ecology* 2003;**84**:511–525.

589 Baker MJ, Trevisan J, Bassan P, Bhargava R, Butler HJ, Dorling KM, Fielden PR, Fogarty SW,
590   Fullwood NJ, Heys KA, *et al.* Using Fourier transform IR spectroscopy to analyze biological
591   materials. *Nat Protoc* 2014;**9**:1771–1791.

592 Balaban B, Urman B. Effect of oocyte morphology on embryo development and implantation.
593   *Reprod Biomed Online* 2006;**12**:608–615.

594 Balaban B, Urman B, Sertac A, Alatas C, Aksoy S, Mercan R. Oocyte morphology does not affect
595   fertilization rate, embryo quality and implantation rate after intracytoplasmic sperm injection.
596   *Hum Reprod* 1998;**13**:3431–3433.

597 Borini A, Bafaro MG, Bianchi L, Violini F, Bonu MA, Flamigni C. Oocyte donation programme:
598   results obtained with intracytoplasmic sperm injection in cases of severe male factor infertility
599   or previous failed fertilization. *Hum Reprod* 1996;**11**:548–550.

600 Borup R, Thuesen LL, Andersen CY, Nyboe-Andersen A, Ziebe S, Winther O, Grøndahl ML.
601   Competence Classification of Cumulus and Granulosa Cell Transcriptome in Embryos
602   Matched by Morphology and Female Age. *PLoS One* 2016;**11**:e0153562.

603 Broekmans FJ, Soules MR, Fauser BC. Ovarian Aging: Mechanisms and Clinical Consequences.
604   *Endocr Rev* 2009;**30**:465–493.

605 Brower PT, Schultz RM. Intercellular communication between granulosa cells and mouse oocytes:
606   Existence and possible nutritional role during oocyte growth. *Dev Biol* 1982;**90**:144–153.

607 Canipari R. Oocyte-granulosa cell interactions. *Hum Reprod Update* 2000;**6**:279–289.

608 Cecconi S, Tatone C, Buccione R, Mangia F, Colonna R. Granulosa cell-oocyte interactions: The

609   phosphorylation of specific proteins in mouse oocytes at the germinal vesicle stage is

610   dependent upon the differentiative state of companion somatic cells. *J Exp Zool*

611   1991;**258**:249–254.

612 Chronowska E. High-throughput analysis of ovarian granulosa cell transcriptome. *Biomed Res Int*

613   2014;**2014**:. Hindawi Publishing Corporation.

614 Cobo A, Kuwayama M, Pérez S, Ruiz A, Pellicer A, Remohí J. Comparison of concomitant

615   outcome achieved with fresh and cryopreserved donor oocytes vitrified by the Cryotop

616   method. *Fertil Steril* 2008;**89**:1657–1664.

617 Colonna R, Cecconi S, Tatone C, Mangia F, Buccione R. Somatic cell-oocyte interactions in mouse

618   oogenesis: Stage specific regulation of mouse oocyte protein phosphorylation by granulosa

619   cells. *Dev Biol* 1989;**133**:305–308.

620 D'Aurora M, Sperduti S, Emidio G Di, Stuppia L, Artini PG, Gatta V. Inside the granulosa

621   transcriptome. *Gynecol Endocrinol* 2016;**32**:951–956. Informa UK Limited, trading as Taylor

622   8 Francis Group.

623 Dumesic DA, Meldrum DR, Katz-Jaffe MG, Krisher RL, Schoolcraft WB. Oocyte environment:

624   Follicular fluid and cumulus cells are critical for oocyte health. *Fertil Steril* 2015;**103**:303–

625   316. Elsevier Inc.

626 Dunning KR, Russell DL, Robker RL. Lipids and oocyte developmental competence: The role of

627   fatty acids and β-oxidation. *Reproduction* 2014;**148**:.

628 Eppig JJ. Intercommunication between mammalian oocytes and companion somatic cells.

629   *BioEssays* 1991;**13**:569–574.

630 Gannon AM, Stämpfli MR, Foster WG. Cigarette Smoke Exposure Elicits Increased Autophagy

631   and Dysregulation of Mitochondrial Dynamics in Murine Granulosa Cells. *Biol Reprod*

632   2013;**88**:63.

633 Gilchrist RB, Lane M, Thompson JG. Oocyte-secreted factors: Regulators of cumulus cell function

634   and oocyte quality. *Hum Reprod Update* 2008;**14**:159–177.

635 Gioacchini G, Giorgini E, Vaccari L, Ferraris P, Sabbatini S, Bianchi V, Borini A, Carnevali O. A

636   new approach to evaluate aging effects on human oocytes: Fourier transform infrared imaging

637   spectroscopy study. *Fertil Steril* 2014;**101**:120–127. Elsevier Inc.

638 Giorgini E, Gioacchini G, Sabbatini S, Conti C, Vaccari L, Borini A, Carnevali O, Tosi G.

639   Vibrational characterization of female gametes: a comparative study. *Analyst* 2014;**139**:5049–

640   5060. Royal Society of Chemistry.

641 González-Fernández R, Peña Ó, Hernández J, Martín-Vasallo P, Palumbo A, Ávila J. FSH receptor,

642   KL1/2, P450, and PAPP genes in granulosa-lutein cells from in vitro fertilization patients show

643   a different expression pattern depending on the infertility diagnosis. *Fertil Steril* 2010;**94**:99–

644   104.

645   Guerif F, Lemseffer M, Leger J, Bidault R, Cadoret V, Chavez C, Gasnier O, Saussereau MH,

646   Royere D. Does early morphology provide additional selection power to blastocyst selection

647   for transfer? *Reprod Biomed Online* 2010;**21**:510–519. Reproductive Healthcare Ltd.

648   Haas J, Ophir L, Barzilay E, Yerushalmi GM, Yung Y, Kedem A, Maman E, Hourvitz A. GnRH

649   Agonist vs. hCG for Triggering of Ovulation – Differential Effects on Gene Expression in

650   Human Granulosa Cells. *PLoS One* 2014;**9**:e90359.

651   Hamamah S, Matha V, Berthenet C, Anahory T, Loup V, Dechaud H, Hedon B, Fernandez A,

652   Lamb N. Comparative protein expression profiling in human cumulus cells in relation to

653   oocyte fertilization and ovarian stimulation protocol. *Reprod Biomed Online* 2006;**13**:807–814.

654   Harper J, Cristina Magli M, Lundin K, Barratt CLR, Brison D. When and how should new

655   technology be introduced into the IVF laboratory? *Human Reproduction* 2012;**27**:303–313.

656   Kidder GM, Vanderhyden BC. Bidirectional communication between oocytes and follicle cells:

657   ensuring oocyte developmental competence. *Can J Physiol Pharmacol* 2010;**88**:399–413.

658   Kim E, Seok HH, Lee S-Y, Lee DR, Moon J, Yoon TK, Lee WS, Lee K-A. Correlation between

659   Expression of Glucose Transporters in Granulosa Cells and Oocyte Quality in Women with

660   Polycystic Ovary Syndrome. *Endocrinol Metab* 2014;**29**:40–47.

661   Kordus RJ, LaVoie HA. Granulosa cell biomarkers to predict pregnancy in ART: pieces to solve the

662   puzzle. *Reproduction* 2017;**153**:R69–R83.

663   La Fuente R De, Eppig JJ. Transcriptional activity of the mouse oocyte genome: companion

664   granulosa cells modulate transcription and chromatin remodeling. *Dev Biol* 2001;**229**:224–236.

665   Matthäus C, Bird B, Miljković M, Chernenko T, Romeo M. Infrared and Raman Microscopy in

666   Cell Biology. *Methods Cell Biol* 2008;**89**:275–308.

667   Movasaghi Z, Rehman S, Rehman I. Fourier Transform Infrared (FTIR) Spectroscopy of Biological

668   Tissues. *Appl Spectrosc Rev* 2008;**43**:134–179.

669   Patrizio P, Sakkas D. From oocyte to baby: a clinical evaluation of the biological efficiency of in

670   vitro fertilization. *Fertil Steril* 2009;**91**:1061–1066.

671   Ruvolo G, Fattouh RR, Bosco L, Brucculeri AM, Cittadini E. New molecular markers for the

672   evaluation of gamete quality. *J Assist Reprod Genet* 2013;**30**:207–212.

673   Sadeu JC, Foster WG. The cigarette smoke constituent benzo[a]pyrene disrupts metabolic enzyme,

674   and apoptosis pathway member gene expression in ovarian follicles. *Reprod Toxicol*

675   2013;**40**:52–59.

676   Serhal PF, Ranieri DM, Kinis A, Marchant S, Davies M, Khadum IM. Oocyte morphology predicts

677   outcome of intracytoplasmic sperm injection. *Hum Reprod* 1997;**12**:1267–1270.

678 Suh CS, Sonntag B, Erickson GF. The ovarian life cycle: A contemporary view. *Rev Endocr Metab*

679   *Disord* 2002;**3**:5–12.

680 Tarín JJ, García-Pérez MA, Cano A. Assisted reproductive technology results: Why are live-birth

681   percentages so low? *Mol Reprod Dev* 2014;**81**:568–583.

682 Tatone C, Amicarelli F. The aging ovary - The poor granulosa cells. *Fertil Steril* 2013;**99**:12–17.

683   Elsevier Inc.

684 Uyar A, Torrealday S, Seli E. Cumulus and granulosa cell markers of oocyte and embryo quality.

685   *Fertil Steril* 2013;**99**:979–997. American Society for Reproductive Medicine.

686 Veeck L, Zaninović N. *An Atlas of Human Blastocyst*. *Parthenon Publ Gr* 2003; CRC Press

687   Company: Boca Raton, London, New York, Washington, D.C.

688 Vergouw CG, Botros LL, Judge K, Henson M, Roos P, Hanna Kostelijk E, Schats R, Twisk JWR,

689   Hompes PGA, Sakkas D, *et al.* Non-invasive viability assessment of day-4 frozen–thawed

690   human embryos using near infrared spectroscopy. *Reprod Biomed Online* 2011;**23**:769–776.

691 Wolkers WF, Oldenhof H. In situ FTIR studies on mammalian cells. *Spectroscopy* 2010;**24**:525–

692   534.

693

694

695

696 **Figure legends**

697 **Figure 1** The methodological process followed in the study.

698 Granulosa cells (GCs) were collected from single-follicle aspirates and retrospectively classified

699 according to companion oocyte clinical outcomes (**CP**, GCs from oocytes, which gave clinical

700 pregnancy; **FF**, GCs from oocytes, which failed fertilization; **EDF**, GCs from oocytes, which failed

701 embryo development, and **IF**, GCs from oocytes, which failed implantation). GCs samples were

702 analysed by Fourier transform infrared microspectroscopy (FTIRM) and the obtained spectral data

703 were then submitted to biomarker signature determination. The selected biomarkers were

704 statistically validated and the macromolecular characterization of GCs was performed.

705 FDA: factorial discriminant analysis, CAP: canonical analysis of principal co-ordinates,

706 PERMANOVA: permutational multivariate ANOVA

707

708 **Figure 2.** Results of factorial discriminant analysis.

709 **(A)** FDA correlation chart showing the correlation of each biomarker with F1 and F2 factors. F1

710 and F2 have 62.75% and 24.14% of discrimination percentage, respectively, for a cumulative

711 percentage of 86.887%.

712 Lipids/overall cellular biomolecular content (LIP/CELL), Proteins/overall cellular biomolecular

713 content (PRT/CELL), AmideI/AmideII (AI/AII), Liids/Protiens (LIP/PRT), Phospahate 1/ overall

714 cellular biomolecular content (PH1/CELL), Phospahate 1/Proteins (PH1/PRT), Carbonyl ester of

715 fatty acids/ overall cellular biomolecular content (COO/CELL), Carbonyl ester of fatty acids/Lipids

716 (COO/LIP), 1400/Proteins 1400/PRT, 1460/Proteins (1460/PRT), 1400/1460, 1460/Lipids

717 (1460/LIP), Unsaturated alkyl chains of lipids/ overall cellular biomolecular content (CH/CELL),

718 Unsaturated alkyl chains of lipids/Lipids (CH/LIP), Unsaturated alkyl chains of lipids/ Methyl

719 groups of cellular lipids (CH/CH3), Methylene groups of cellular lipids/Lipids (CH2/LIP), and

720 Methyl groups of cellular lipids/ Methylene groups of cellular lipids (CH2/CH3). **(B)** Two-

721 dimensional chart showing the classification of the observations by FDA plotted on the F1 and F2

722 factors, with a cumulative discrimination percentage of 86.887.

723

724 **Figure 3** Results of canonical analysis of principal coordinates.

725

726 Canonical analysis of principal coordinates (CAP) plot showing the constrained ordination of the

727 observations plotted on the CAP1 and CAP2 axes, with vector overlay of Spearman rank

728 correlations of each biomarkers with CAP axes.

729

730 **Figure 4**. Results of ANOVA test**.**

731 Box charts show the values of the 17 biomarkers for each experimental group: centre line marks the

732 median, edges indicate the 25th and 75th percentile, whiskers indicate the 5th and the 95th percentile,

733 the black square marks the mean, black circles indicate the minimum and maximum values,

734 coloured diamonds indicate the outliers. Different letters above box charts indicate a statistically

735 significant difference among groups Statistical significance was set at 0.05, and calculated by

736 ANOVA followed by Dunnett's multiple comparisons test.

737

738

739

740

741

742

743

744

Spectral Interval (cm^{-1})	Vibrational attribution	Label	Cellular features	Reference
2990−2836	Symmetric and asymmetric CH$_{2/3}$ stretching modes	**Lipids**	Saturated alkyl chains of cellular lipids (mainly) and proteins	(Baker *et al.*, 2014)
3027-2995	=CH stretching mode	**CH**	Unsaturated alkyl chains of lipids	(Giorgini *et al.*, 2014)
2992−2948	Asymmetric CH$_3$ stretching mode	**CH$_3$**	Methyl groups of cellular lipids (mainly) and proteins	(Sabbatini *et al.*, 2013)
2946−2889	Asymmetric CH$_2$ stretching mode	**CH$_2$**	Methylene groups of cellular lipids (mainly) and proteins	(Sabbatini *et al.*, 2013)
1765-1723	C=O ester moiety stretching	**COO**	Carbonyl ester of fatty acids	(Gioacchini *et al.*, 2014)
1723-1591	Mainly C=O stretching in peptide linkage, Amide I	**AI**	Cellular proteins	(Baker *et al.*, 2009)
1591−1481	Mainly C-N stretching and N-H deformation in peptide linkage, Amide II, **AII**	**AII**		
1723-1481	Sum of **AI** and **AII**, **Proteins**	**Proteins**		
1480-1426	CH$_{2/3}$ bending	**1460**	Methyl and methylene groups of cellular lipids (mainly) and proteins	(Conti *et al.*, 2007)
1426-1372	Mainly CH$_3$ symmetric stretching of protein chains	**1400**	Methyl groups of cellular lipids (mainly) and proteins	(Caine *et al.*, 2012)
1273-1191	Asymmetric stretching modes of phosphate groups	**Ph1**	Phosphate moieties of nucleic acids (mainly), phospholipids and phosphorylated proteins	(Giorgini *et al.*, 2015; Tosi *et al.*, 2010)
2990−2899 & 1775−1191	Sum of all the vibrations indicated above	**Cell**	Overall cellular biomolecular content	

745 **Table I** Spectral intervals of the main bands comprising granulosa cell infrared spectra, together

746 with the related vibrational mode, assigned label, and the cellular functional groups.

747

748

Band area ratios	Label	Biological significance
Lipids/Cell	LIP/CELL	Total cellular lipids
Proteins/Cell	PRT/CELL	Total cellular proteins
AmideI/AmideII	AI/AII	Protein pattern
Lipids/Proteins	LIP/PRT	Lipids related to protein content
Phosphate1/Cell	PH1/CELL	Total cellular phosphate groups
Phosphate1/Proteins	PH1/PRT	Phosphate groups related to protein content
Phosphate1/Lipids	PH1/LIP	Phosphate groups related to lipid content
Carbonyl ester of fatty acids /Cell	COO/CELL	Total cellular fatty acids
Carbonyl ester of fatty acids /Lipids	COO/LIP	Ester moieties in lipids
1400/Proteins	1400/PRT	Methyl groups related to protein content
1400/Lipids	1400/LIP	Methyl groups related to lipid content
1460/Proteins	1460/PRT	Methyl and methylene groups related to protein content
1400/1460	1400/1460	Methyl and methylene proportion in aliphatic chains
1460/Lipids	1460/LIP	Methyl and methylene groups related to lipid content

Unsaturated alkyl chains of lipids /Cell	CH/CELL	Unsaturation levels in lipid chains
Unsaturated alkyl chains of lipids /Lipids	CH/LIP	
Unsaturated alkyl chains of lipids / Methyl groups of cellular lipids	CH/CH3	
Methylene groups of cellular lipids /Lipids	CH2/LIP	Branching of lipid chains
Methylene groups of cellular lipids / Methyl groups of cellular lipids	CH2/CH3	

749

750   **Table II** Band area ratios calculated on the spectral intervals defined in Table I with their assigned

751   label and biological significance.

752

753

754

755

756   **Table III** Pair-wise permutational multivariate ANOVA results.

757
758

Groups	t	P(perm)	Unique perms	P(MC)
CP, IF	8.0024	0.001	999	0.001
CP, FF	4.2377	0.001	997	0.001
CP, EFD	4.9418	0.001	999	0.001
IF, FF	5.5322	0.001	999	0.001
IF, EDF	5.6797	0.001	997	0.001
FF, EDF	2.8348	0.001	998	0.001

759
760

761 Results reported as: *t*, pseudo-*t*, calculated as the square root of pseudo-*F*; *P(perm)*, permutation P value;

762 *P(MC)*, Monte Carlo P-value.

763 CP, Granulosa cells (GCs) from oocytes, which gave clinical pregnancy; FF, GCs from oocytes, which failed

764 fertilization; EDF, GCs from oocytes, which failed embryo development, and IF, GCs from oocytes, which

765 failed implantation.

766

767

768 **Table IV** The confusion matrix for the estimation sample.

769

from \ to	CP	FF	EDF	IF	Total	% correct
CP	207	47	12	24	290	71.38%
FF	13	243	12	18	286	84.97%
EDF	0	22	177	1	200	88.50%
IF	30	26	1	210	267	78.65%
Total	250	338	202	253	1043	80.25%

770

771 The matrix reports the reclassification of the observations, and shows the percentage of well classified

772 observations, calculated by dividing the number of well classified observations by the total number of

773 observations.

774

775

776

777 **Table V** The confusion matrix for cross-validation of results.

778

from \ to	CP	FF	EDF	IF	Total	% correct
CP	16	3	3	1	23	69.565%
FF	2	19	1	1	23	82.609%
EDF	0	2	21	0	23	91.304%
IF	3	3	0	17	23	73.913%
					Total	79.348%

779

780 The matrix reports the leave-one-out allocation of observations to experimental groups, and shows the

781 percentage of well classified observations, calculated by dividing the number of well classified observations

782 by the total number of observations.

783

784

785

786

787

GCs from single follicles

Retrospective classification

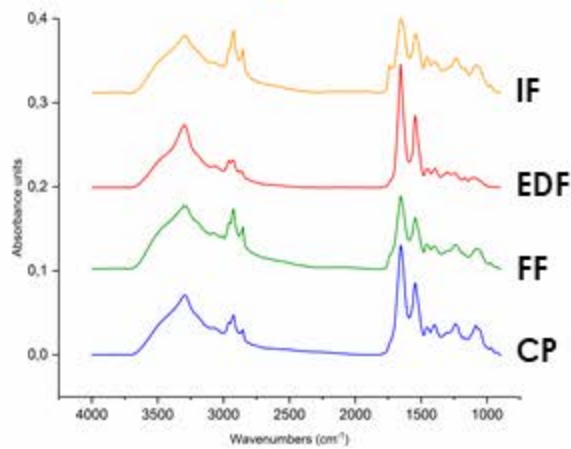FF: fertilization failure   EDF: embryo development failure

IF: implantation failure   CP: clinical pregnancy

FTIRM data collection

Biomarker signature

Biomarker validation   Macromolecular characterization of GCs

PERMANOVA
FDA
CAP

ANOVA

A

B

Observations (F1 and F2: axes 86.89 %)